



**ORIGINAL ARTICLE**

## Parametric design of developable structure based on Yoshimura origami pattern

Haolei Jiang<sup>a</sup>, Wen Liu<sup>a,\*</sup>, Haoyu Huang<sup>b</sup>, Yiqin Wang<sup>a</sup>

<sup>a</sup> Department of Civil Engineering, Beijing Forestry University, Beijing 100083, China.

<sup>b</sup> School of Engineering, Newcastle University, Newcastle upon Tyne NE1 7RU, UK.

\*Corresponding Author: Wen Liu. Email: liuwen@bjfu.edu.cn.

**Abstract:** Origami is an ancient art form and can be divided into rigid and non-rigid origami. Rigid origami is suitable for the design of building structures because the panels are not twisted and deformed during the folding process. Currently, rigid origami structures are generally built with steel. However, compared with natural, non-polluting wood, steel has a high energy consumption and a high environmental impact. Based on this situation, this paper designs a developable wooden building structure using the Yoshimura origami model. First, the Jacobian matrix method was used to analyze the degree of freedom of the basic unit of the Yoshimura origami pattern, following which the motion trajectory required by the target structure was obtained. Secondly, by analyzing the relationship between the plane angle  $\alpha$  and dihedral angle  $\theta$ , three interaction rules were obtained, and the formula for determining the structure size was established by using the plane angle  $\alpha$ , dihedral angle  $\theta$ , the number of valley folds  $n$  and the unit length  $l$ . Subsequently, two enhancement schemes, the quadrangle enhancement scheme and the triangle enhancement scheme, were proposed to increase the height of the structure. After comparing the deformation and failure types of origami structures based on Cross-Laminated Timber, a triangular reinforcement scheme was chosen to increase the height of the structure. Finally, a new connection method was developed that allowed the origami structure to be practically applied. This research demonstrates the possibility of developing a timber structure based on Yoshimura origami.

**Keywords:** Yoshimura origami pattern; degree of freedom; cross-laminated timber; structure deformation; enhancement scheme; connection hinge

### 1 Introduction

Origami is an ancient art form in East Asia. It creates various three-dimensional (3D) handicrafts by simply folding a flat piece of paper without shearing, adhesion, or external support. Modern origami originated in Japan. Origami was originally considered as art or decoration. Until the end of the 19th century, the first international scholarly conference on origami was held, scholars began to explore origami's scientific principles and apply them to large-scale projects. In practice, such projects were primarily based on rigid origami. It can be described as a panel-hinge framework formed by rigid panels without self-intersection [1]. Rigid origami only features valley folds (**Fig. 1a**) and mountain folds (**Fig. 1b**); other types of deformations, such as bending, tension, and compression, do not occur on the surface between creases [2]. Nowadays, rigid origami had been used in various industries, and it was



particularly useful in the space industry, where large panels must be frequently transported to space. For example, Robert Lang was the first person to successfully send the Eyeglass space telescope into space by folding it into a suitable shape based on the principles of rigid origami [3]. In medicine, Knribayashi et al. combined a rigid origami structure with circular tubes and developed a self-expanding surgical stent that could be propped open at a predetermined position to recirculate blood [4].

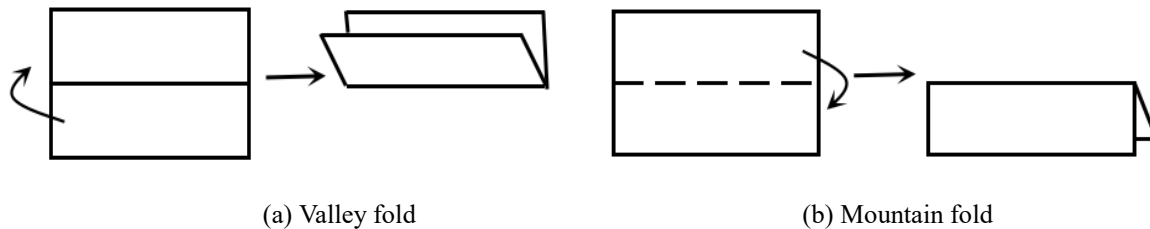


**Fig. 1.** Two approaches of rigid origami

Rigid origami is classified according to its crease forms. Classical forms include the Miura-ori origami pattern proposed by Koryo Miura in 1972 [5] and the Huffman grid origami pattern proposed by David Huffman in 1976 [6]. These rigid origami patterns have been used to design architectural structures. The Huffman grid origami pattern was used in the roof of a sketch building at the Hanover World Expo in 2000 and for the gate of the 2002 Turin Winter Olympics. Stavric et al. [7] constructed an architectural sketch using the expansion pattern of Miura-ori origami and analyzed the bearing capacity of the structure by using finite element software. Falk et al. [8] designed a temporary church in Saint Loup, France, and optimized the lighting of the building through Autodesk Ecotect Analysis software, which was also based on the Miura-ori origami pattern. The Yoshimura origami pattern was proposed by Yoshimura in 1955, in which Yoshimura observed that under axial compression, the thin-walled cylindrical tube structure produced a specific pattern on the surface of the tube. Many studies on this pattern were conducted by domestic and foreign scholars, though most of them were about round tubes. For example, Pellegrino et al. [9-11] designed a spiral-style rigid folded pipe and analyzed the relationship among the side lengths, angles, and creases, and they established a parametric model of the folded circular pipe. Hunt et al. [12] developed a torsional folding structure and determined the relationship among parameters by twisting a thin-paper circular tube. Yang et al. [13-14] designed an octagonal tubular folded structure (**Fig. 2**). The height of the tubular structure was calculated using geometric parameters, such as side length and folded dihedral angle. They also employed multi-objective optimization to study the influence of parameters, such as folding dihedral angle, folding side length, and height, on the energy absorption capacity of the tube structure. They used brass as the material and 3D printed the tubular folding structure. Yan et al. [15-16] from Tianjin University in China, also designed a tubular folding structure and studied the influence of various geometric parameters on the height and energy absorption characteristics of the tubular structure. Shen et al. [17] analyzed the effect of different design parameters on the radial stiffness of the new thin-walled tubular structure using Yoshimura and modified Yoshimura origami patterns as a framework. In recent years, Yoshimura Origami structures were also developed greatly in the field of robotics. For example, soft body creeping crawling robot [18], earthworm-like planar locomotion robot [19]. In terms of architecture, Heike Matcha et al. [20] instructed students to use corrugated cardboard to build temporary buildings based on Yoshimura origami pattern and used Grasshopper scripts to design market halls and shelters; Hani Buri et al. [21] and local architects in Lausanne designed an origami-style chapel built of wooden boards.

In terms of architectural structures, the Yoshimura origami pattern was better than other origami patterns. For example, the Miura-ori origami pattern could only be used to form a flat structure, and it could bear only a small vertical load. Variants of the Miura-ori origami pattern could be used with the Huffman grid pattern to form an arch and to resist vertical loads; however, the basic unit was quadrilateral, which was not as stable as a triangular unit and was as inerratic as the arch structure formed using the Yoshimura origami pattern.

Currently, green construction materials are widely concerned, and there is increasing resistance to heavy polluting materials such as steel and concrete. Cross-laminated timber (CLT) is a sustainable wood material that can obviously reduce carbon emissions to the environment and has mechanical properties that meet the requirements for building use. By going through a lot of literature, it is found

that origami structure buildings seldom use wood material. So this paper will design origami structure using CLT material and hope it can provide a boost to the development of origami structures.

The parametric design was proposed as the ideal powerful method for modelling Origami structures, applicable in both geometrical and analysis processes [22].The following studies were conducted to apply Yoshimura origami patterns to the design of architectural structures. Firstly, the degrees of freedom (DOFs) of each vertex of the Yoshimura origami pattern were analyzed, and equations were used to simplify the DOFs and facilitate structural calculation. Subsequently, the relationships between parameters such as the plan angle, dihedral angle, span, and height of the structure were determined. Building structures with different size requirements were then designed according to the formulas. Finally, two variants of the Yoshimura origami pattern were proposed to increase the height of the structure by modifying the crease scheme, after which the deformation of the structure was analyzed. Accordingly, the scheme that was better for increasing the structure height was chosen.

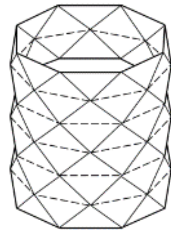


Fig. 2. Octagonal tubular folding structure

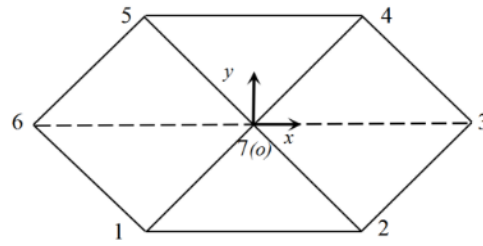


Fig. 3. Yoshimura origami pattern

## 2 DOFs analysis of Yoshimura origami pattern with single vertex

A basic unit of the Yoshimura origami pattern is shown in Fig. 3. The unit comprises isosceles triangles. Each vertex corresponds to six creases, which include two valley folds and four mountain folds. The Yoshimura origami pattern has more folds than the Miura-ri origami pattern, so there are more DOFs and more complex movements.

In this paper, the Jacobian matrix method [23] was used to calculate DOFs. Rigid constraints, boundary constraints, and connection constraints were applied to the rigid units in this method; the constraints of the entire system could be determined. After determining these constraints, Eq. (1) could be obtained:

$$f_j(x_1, x_2, \dots, x_n, y_1, y_2, \dots, y_n, z_1, z_2, \dots, z_n) = 0 \tag{1}$$

$j = 1, 2, \dots, m$ , where  $m$  is the number of constraint equations,  $n$  is the number of nodes in the origami pattern, and  $x_n, y_n,$  and  $z_n$  are the coordinate values of the nodes. Differentiating the system constraint equations with respect to time yield the Jacobian matrix, the rank of the Jacobian matrix could then be obtained. The rank represents the number of effective constraints, and the number of DOFs of the origami pattern could be obtained by subtracting the rank from the number of unknowns.

Table 1. Node coordinates of single-vertex Yoshimura origami pattern

| The number of nodes | 1                    | 2                     | 3          | 4                    | 5                     | 6           | 7 |
|---------------------|----------------------|-----------------------|------------|----------------------|-----------------------|-------------|---|
| $x$                 | $\frac{\sqrt{2}}{2}$ | $\frac{\sqrt{2}}{2}$  | $\sqrt{2}$ | $\frac{\sqrt{2}}{2}$ | $-\frac{\sqrt{2}}{2}$ | $-\sqrt{2}$ | 0 |
| $y$                 | $\frac{\sqrt{2}}{2}$ | $-\frac{\sqrt{2}}{2}$ | 0          | $\frac{\sqrt{2}}{2}$ | $\frac{\sqrt{2}}{2}$  | 0           | 0 |
| $z$                 | 0                    | 0                     | 0          | 0                    | 0                     | 0           | 0 |

### 2.1 Rigid constraints

The Yoshimura origami pattern comprises triangles. The rigid constraints of triangular plates were analyzed as follows. First, the nodes in the graph were numbered counterclockwise from 1 to 6, and the vertices were numbered 7. The Cartesian coordinated system was used, and 7 (o) was set at the vertex. Assuming that the triangle was an isosceles right-angled triangle, the waist length was 1, that was,  $l_{16} = l_{17} = l_{56} = l_{57} = l_{27} = l_{23} = l_{47} = l_{43} = 1$ , the coordinates of each node areas listed in Tab. 1.

The pattern comprises six triangular rigid plates, namely plates 1-2-7, 2-3-7, 3-4-7, 4-5-7, 5-6-7, and 1-7-6. The shape of a rigid triangle could be bounded by the lengths of the three sides determined as constants. Eq. (2) was used to determine the length of each side, as follows

$$\begin{cases} (x_1-x_2)^2+(y_1-y_2)^2+(z_1-z_2)^2=l_{12}^2 \\ (x_2-x_7)^2+(y_2-y_7)^2+(z_2-z_7)^2=l_{27}^2 \\ (x_7-x_1)^2+(y_7-y_1)^2+(z_7-z_1)^2=l_{71}^2 \\ \dots \\ (x_6-x_1)^2+(y_6-y_1)^2+(z_6-z_1)^2=l_{61}^2 \end{cases} \quad (2)$$

Correspondingly, a rigid constraint condition of the triangular rigid plate was obtained as that  $l_{12}$ ,  $l_{27}$ ,  $l_{71}$ ,  $l_{23}$ ,  $l_{37}$ ,  $l_{34}$ ,  $l_{47}$ ,  $l_{45}$ ,  $l_{57}$ ,  $l_{56}$ ,  $l_{67}$  and  $l_{61}$  were all constants.

### 2.2 Boundary constraints

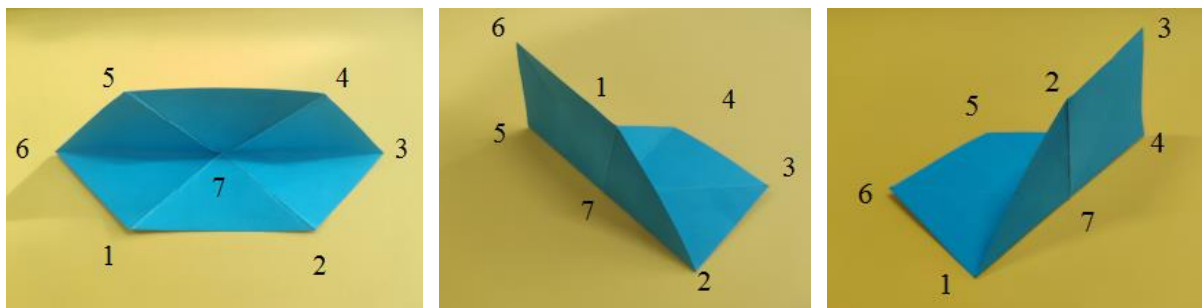
The rigid constraint of the plate was determined, after which the boundary constraint conditions of the plate were analyzed to avoid global displacement and rotation. Only the vertex had to be constrained because each triangle had a common vertex. Correspondingly, the boundary constraint was obtained as that  $x_7$ ,  $y_7$  and  $z_7$  were constants.

### 2.3 Connection constraints

After the rigid constraints and boundary constraints of the rigid plates were obtained, the connection constraints between the rigid plates were analyzed. The connection constraint between rigid plates was regarded as a spherical joint constraint. A spherical joint had a large range of motion, high flexibility, and a rich attitude. The constraints corresponding to the spherical joints were automatically satisfied when adjacent plates share a common point. Therefore, the connection constraints naturally met the conditions due to the structural constraints in the motion, and there was no need to set additional constraint equations.

### 2.4 Single vertex Yoshimura origami pattern Jacobi matrix

The rigid and boundary constraints in the above analysis were used to solve the Jacobian matrix of the Yoshimura origami pattern. Because there were 15 constraint equations and 21 variable parameters in 7 nodes, so a  $15 \times 21$  Jacobian matrix was obtained. The Jacobi matrix was input into MATLAB, and the matrix rank was calculated to be 15; in other words, the number of DOFs was six, which was inconsistent with the theory that a single vertex with six creases had three DOFs. By observing the Yoshimura origami pattern, it was found that the reason was the pattern could be folded around valley folds 3-6 and mountain folds 2-5 and 1-4 (Fig. 4a, b, c). To exclude these three types of motion, it was judged that  $l_{36}$ ,  $l_{25}$  and  $l_{14}$  in Eq. (2) were not constants, which could prevent the 6 triangular rigid plates from being coplanar during motion and to allow the number of DOFs to be reduced to 3.



(a) Around the valley 3-6 (b) Around the mountain 2-5 (c) Around the mountain 1-4

**Fig. 4.** Motion of folding around the valley fold 3-6 and the mountain folds 2-5 and 1-4

For parameter design and the building structure, the 3-DOFs movement was still highly complex, the expected structure was difficult to obtain in the absence of constraints. A further observation of the single-vertex Yoshimura origami pattern revealed that the three irregular folding motions shown in Fig.

5 were not allowed, which indicated that boundaries 1-2 and 4-5 could not be kept parallel with the initial condition. Therefore, Eq. (3) could be used to eliminate the three irregular folding motions.

$$y_1 = y_2, y_4 = y_5 \tag{3}$$

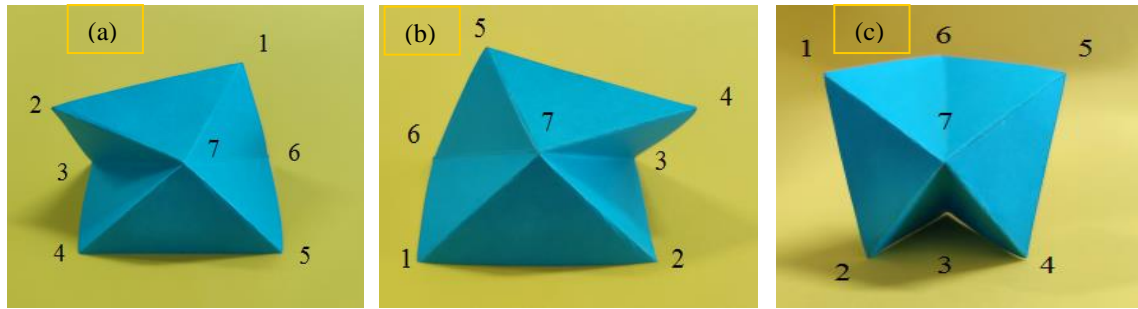
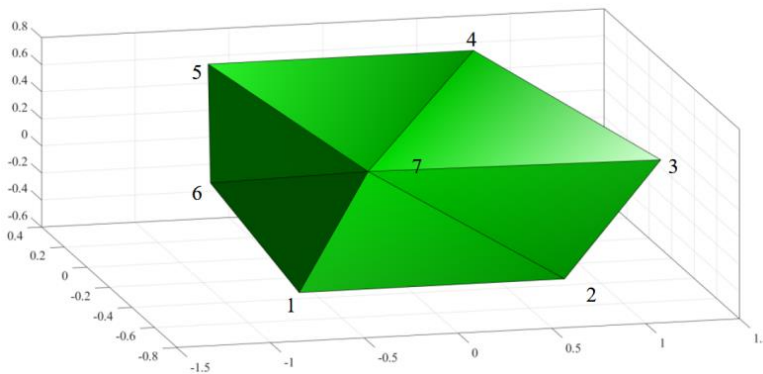


**Fig. 5.** Three irregular folding motions. (a) Boundary 1-2 does not maintain horizontal movement, (b) Boundary 4-5 does not maintain horizontal movement, (c) Boundary 1-2, 4-5 do not maintain horizontal movement

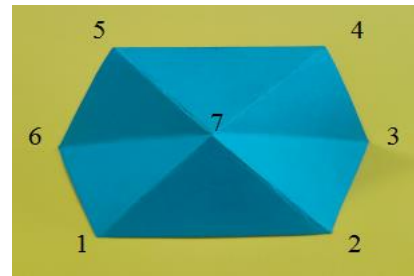
Finally, the Jacobi matrix of a single-vertex Yoshimura origami pattern was obtained, whose calculation result had one DOF. Making the entire unit move by controlling node 3 and using MATLAB to calculate the constraint equations to obtain the coordinates of other nodes when  $x_3 = 1.2$  ( $0 < x_3 < 1.42$ ), The results are listed in **Tab. 2**. Each vertex of the Yoshimura origami pattern could move in accordance with the needed for track motion (**Fig. 6**).

**Table 2.** Node coordinates of single-vertex Yoshimura origami pattern when  $x_3 = 1.2$

| The number of nodes | 1       | 2       | 3       | 4      | 5       | 6       | 7 |
|---------------------|---------|---------|---------|--------|---------|---------|---|
| $x$                 | -0.7071 | 0.7071  | 1.2     | 0.7071 | -0.7071 | -1.2    | 0 |
| $y$                 | -0.5668 | -0.5668 | -0.6004 | 0.242  | 0.242   | -0.6004 | 0 |
| $z$                 | -0.4228 | -0.4228 | 0.4466  | 0.6644 | 0.6644  | 0.4466  | 0 |



(a) Folding sequence simulated in MATLAB



(b) Folding sequence of paper card

**Fig. 6.** Folding motion

**Table 3.** Parameter definition

| Parameter | Definition   | Unit      |
|-----------|--|-----------|
| $\alpha$  | Plane angle between the valley and mountain folds in the crease scheme | degree(°) |
| $\theta$  | Dihedral angle between two adjacent faces during folding               | degree(°) |
| $\beta$   | Introduction angle   | degree(°) |
| $l$       | Length of the long side of the isosceles triangle                      | mm        |
| $n$       | Number of complete valley folds in the crease scheme                   | -         |
| $m$       | Number of repetitions of the basic crease scheme                       | -         |
| $S$       | Span of the entire structure   | mm        |
| $L$       | Length of the entire structure   | mm        |
| $H$       | Height of the entire structure   | mm        |

### 3 Parametric design of Yoshimura origami pattern

The definitions of the parameters used in this section were listed in **Tab. 3**.

#### 3.1 Relationship between plane angle and dihedral angle

Although the crease scheme shown in **Fig. 7a** could fold into a 3D form shown in **Fig. 7b**, the entire folding process still featured some styles which not only depended on the initial creases but also relied on changes in the angle between faces. To make the structure simple and efficient, this paper folded the edge plate to reach the point of moment, which was perpendicular to the horizontal plane, to form the target shape of the structure. In doing so, a stable connection was quickly and easily achieved between the structure and foundation.

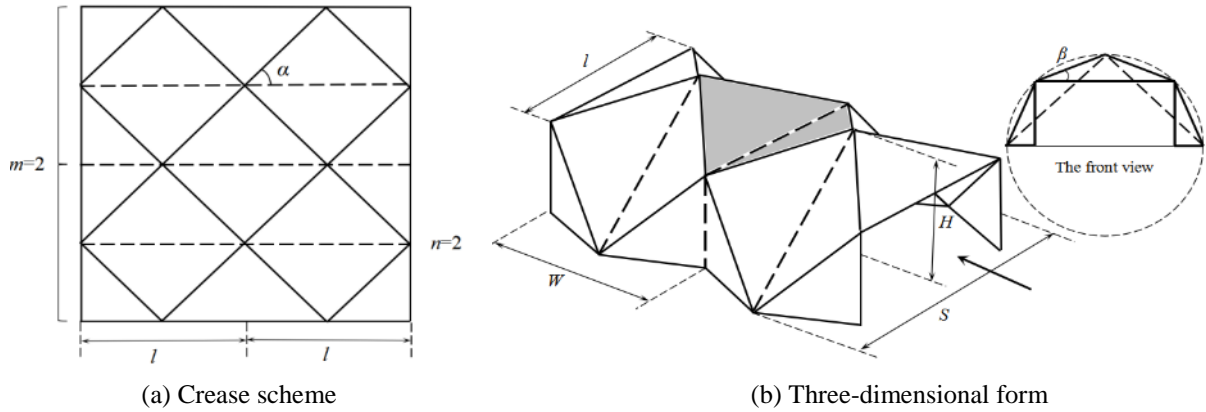


**Fig. 7.** Target structure

The Yoshimura origami crease pattern was determined by the plane angle  $\alpha$  in **Fig. 7a**. The plane angle  $\alpha$  must be  $0 < \alpha \leq \pi/4$  for the pattern to be folded. To obtain the relationship between the plane angle  $\alpha$  and dihedral angle  $\theta$ , the dihedral angle in the shaded part of **Fig. 7b** was neglected in the analysis (**Fig. 8**).

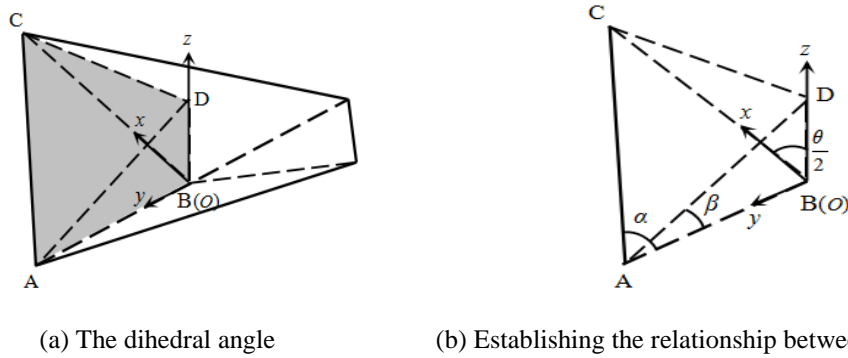


**Fig. 8.** Analysis of the relationship between plane angle  $\alpha$  and dihedral angle  $\theta$

First, the coordinate system  $oxyz$  was established at the diagonal intersection (**Fig. 8a**). The origin  $o$  was set at point  $B$ . The positive  $x$ -axis extended from points  $B$  to  $C$ , the positive  $y$ -axis extended from points  $B$  to  $A$ , and the positive  $z$ -axis extended straight up from point  $B$ .  $Rt\triangle ABD$  (Right-angled triangle  $ABD$ ) was the projection of  $Rt\triangle ABC$  onto the  $yozy$  plane, and  $Rt\triangle CBD$  was obtained by connecting points  $C$  and  $D$ . To establish the relationship between the plane angle  $\alpha$  ( $\angle BAC$ ) and dihedral angle  $\theta$  ( $2\angle CBD$ ), this paper added an introduction angle  $\angle DAB$  denoted  $\beta$ . In **Fig. 8b**,  $\tan(\alpha) = BC/AB$ ,  $\cot(\beta) = AB/BD$ , and  $\sec(\theta/2) = BC/BD$  could be obtained by analyzing  $Rt\triangle ABC$ ,  $Rt\triangle ABD$ , and  $Rt\triangle CBD$ . Thereafter,  $\tan(\alpha) \times \cot(\beta) = \sec(\theta/2)$  was obtained using Eq. (4), where  $\beta$  could be calculated by the number of valley folds, as in Eq. (5).

$$\theta = 2 \operatorname{arcsec}(\cot \beta \times \tan \alpha) \tag{4}$$

$$\beta = \frac{180 - \frac{(4n-2) \times 180}{4n}}{2} \tag{5}$$

The relationship between the plane angle  $\alpha$  and dihedral angle  $\theta$  was drawn in MATLAB (Fig. 9).

1) For the same curve, the dihedral angle  $\theta$  increased with the plane angle  $\alpha$  of the crease pattern. However, this growth rate is gradually decreasing.

2) For the same plane angle  $\alpha$ , increasing the number of valleys led to an increase in the dihedral angle  $\theta$ .

3) For some valleys, the design of plane angle  $\alpha$  was not only limited by the maximum value of  $45^\circ$  but also by the minimum value. For example, in the case of three valleys, if the plane angle  $\alpha$  was  $<22.5^\circ$ , then the pattern was unable to fold into the required structure.

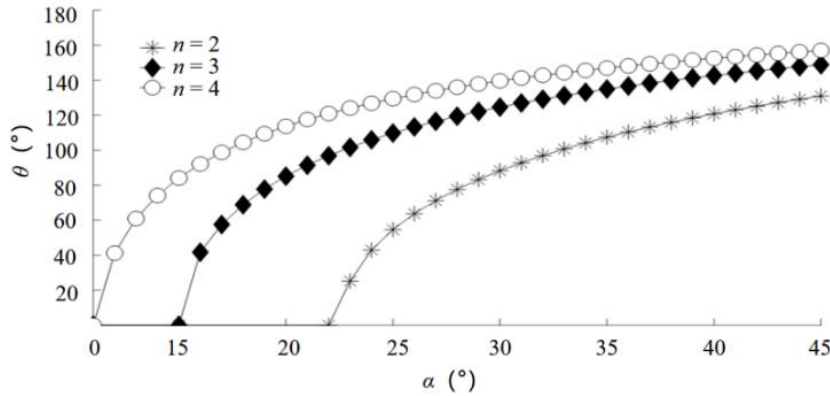


Fig. 9. The relationship between plane Angle  $\alpha$  and dihedral Angle  $\theta$

### 3.2 Parameter design

The plane angled  $\alpha$  and dihedral angle  $\theta$  influence each other, and they affect the final size of the structure. The height  $H$  and span  $S$  of the structure were determined from the front view of the structure. As shown in Fig. 7b, the structure eventually formed a semicircular shape. The inner regular polygon of the semicircle was its outer contour, consequently, Eq. (6)-(8) could be obtained.

$$H = \frac{l}{4 \cos \beta \times \sin(\frac{\pi}{4n})} \tag{6}$$

$$S = 2H \tag{7}$$

$$L = m \times \frac{l}{2} \tan \alpha \times \sin \frac{\theta}{2} \tag{8}$$

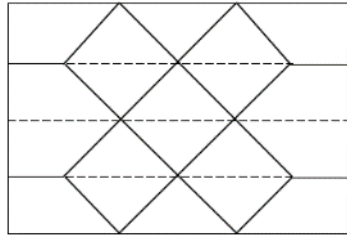
Table 4. Structural dimensions corresponding to different crease schemes

| Parameters             | $\theta$ (°) | $H$ (mm) | $S$ (mm) | $L$ (mm) |
|------------------------|--------------|----------|----------|----------|
| $\alpha=45^\circ, n=2$ | 131.06       | 1760     | 3530     | 1140     |
| $\alpha=30^\circ, n=2$ | 88.31        | 1760     | 3530     | 530      |
| $\alpha=25^\circ, n=2$ | 54.68        | 1760     | 3530     | 270      |
| $\alpha=45^\circ, n=3$ | 148.91       | 2500     | 5000     | 1200     |
| $\alpha=30^\circ, n=3$ | 124.69       | 2500     | 5000     | 640      |
| $\alpha=20^\circ, n=3$ | 85.18        | 2500     | 5000     | 310      |
| $\alpha=45^\circ, n=4$ | 157.05       | 2500     | 6530     | 1220     |
| $\alpha=30^\circ, n=4$ | 139.69       | 2500     | 6530     | 670      |
| $\alpha=15^\circ, n=4$ | 84.13        | 2500     | 6530     | 240      |

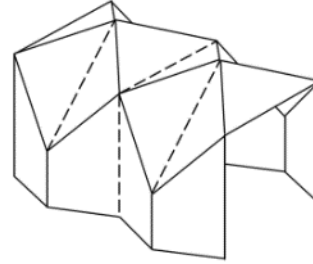
The height and span of the structure were dependent on the sides of the polygon, which was, they were only dependent on the number of valleys folds  $n$  and element length  $l$  in the crease pattern. When the number of valleys folds and element length was determined, the shape of the cross-section could also be determined. The length of the structure was not only dependent on the length of the element but also dependent on the folded state of the structure. Only when the plane angle  $\alpha$  and dihedral angled  $\theta$  were determined could the length of the structure be calculated. The values of the parameters

corresponding to some crease schemes were listed in **Tab. 4**. According to the dimensions and basic modules of wooden plates commonly used in the project, the element length  $l$  was set to 2500 mm.

As listed in **Tab. 4**, the height of the structure was only 1760 mm when  $n = 2$ , which did not conform to the requirements for daily use. Therefore, two solutions were proposed. The first solution involved increasing the height of the structure by changing the element length, for example, the height could reach 2470 mm when the element length  $l$  was 3500mm. The second solution involved increasing the height of the structure by modifying the edge shape of the crease pattern. As a result, two crease schemes were proposed to increase the height of the structure (**Fig. 10** and **Fig. 11**).

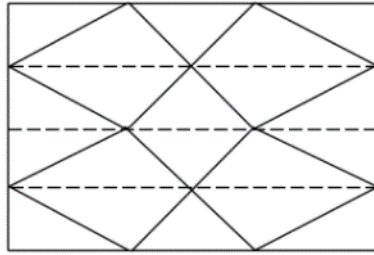


(a) Crease scheme

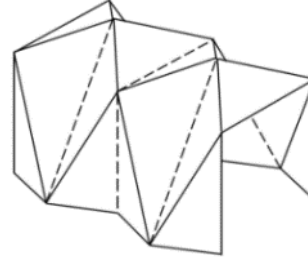


(b) Three-dimensional form

**Fig. 10.** Quadrangle enhancement scheme



(a) Crease scheme



(b) Three-dimensional form

**Fig. 11.** Triangle enhancement scheme

## 4 Structural deformation design

### 4.1 Bar-hinge model

MERLIN2\_v1.1, a dedicated open-source MATLAB code for the structural analysis of origami assemblages, was used to simulate the entire deformation process of the origami structure when subjected to external forces. The bar-hinge model was a highly efficient approach for analyzing origami systems based on reduced-order modeling, which predicted their global mechanical behavior surprisingly well (Fig. 12). The bar-hinge model represented the kinematic space of an origami structure, with a bar (or truss) frame associated with constrained out-of-plane rotations; three fundamental deformation modes in origami were successfully captured using this method: (in-plane) stretching, (out-of-plane) crease folding, and (out-of-plane) panel bending [24]. Bars were placed along straight fold lines and across panels for in-plane stiffness. The rotational hinges were located along the bars connecting panels to model the folding of creases; the rotational hinges were along the bars across panels to model the bending of panels.

Liu and Paulino [25] considered a discretized origami assemblage to be an elastic system. The total potential energy ( $\Pi$ ) of the system included contributions from the bars ( $U_S$ ), bending hinges ( $U_B$ ), and folding hinges ( $U_F$ ). The total potential energy of the system was thus written as,

$$\Pi(u) = U_S(u) + U_B(u) + U_F(u) - f^T(u) \quad (9)$$

Where  $f$  was the externally applied load, and all the other energy terms were nonlinear functions of the nodal displacements  $u$ .

In this paper, the above models and codes were used.

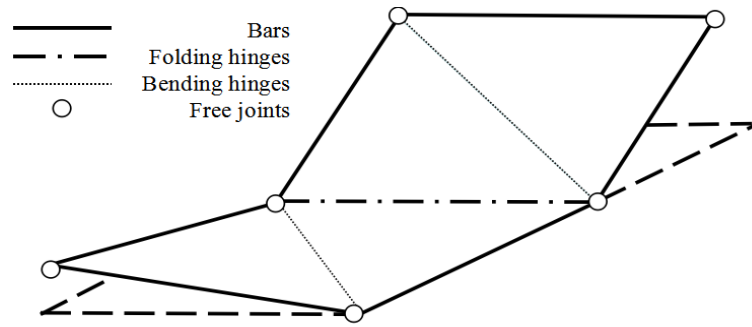


Fig. 12. Bar-hinge model

#### 4.2 Material parameters of CLT

CLT is a new type of green and environment-friendly material made of wood cut into a plate shape and glued by orthogonal stacking. Introduced by Austria and Germany in the early 1990s, the demand for CLT grew worldwide as people began to see and take advantage of its benefits [26]. Wood construction had flourished in the last few decades, and applying CLT to origami structures was a new direction and support for green building.

The mechanical property of CLT was used to analyse the behavior of Yoshimura origami structure. Using MERLIN2\_v1.1 under auto-mode, set the elastic moduli of CLT as  $E = 11$  GPa (major strong direction) and  $E_1 = 13$  GPa (secondary strong direction  $E_2 = 9$  GPa), Poisson's ratio as  $\nu = 0.33$ , material thickness as  $t = 105$  mm (three glued layers of boards), and element length as  $l = 2500$  mm. The structure was loaded by displacement control.

#### 4.3 Structural deformation calculation

Two constraint cases were listed in **Tab. 5**.

Table 5. Number of different bottom constraints

| Scheme                            | All bottom nodes consolidate fully | The bottom nodes consolidate at one end and the other nodes allow $y$ -axis displacement |
|-----------------------------------|------------------------------------|--|
| The quadrangle enhancement scheme | 1-1                                | 2-1  |
| The triangle enhancement scheme   | 1-2                                | 2-2  |

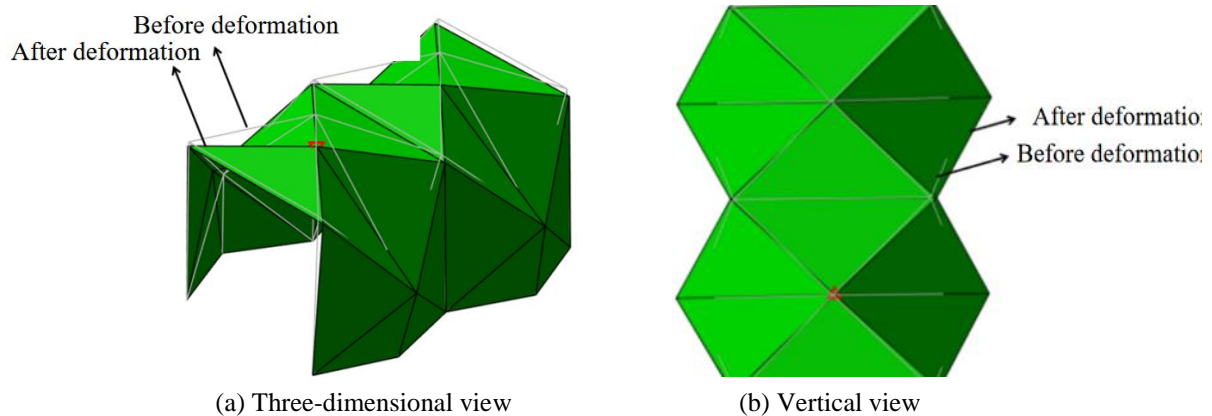
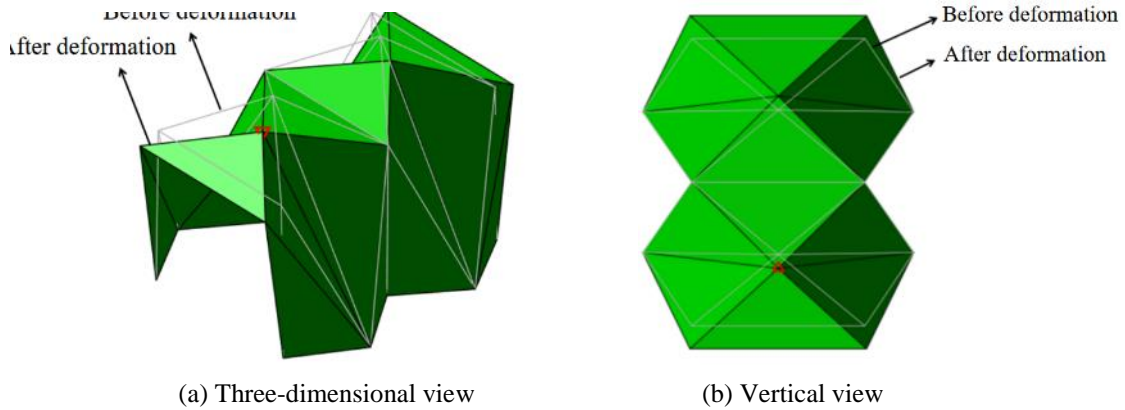


Fig. 13. Overall deformation of 1-1

As shown in **Fig. 13** and **Fig. 14**, the two nodes at the top of the structure were displaced by 0.1 m. The white lines represent the structure before displacement, and the green panels represent the structure after deformation. First, the 3D graphs indicated that the two types of structural deformations completely differed when all bottom nodes were fully consolidated. In the quadrangle enhancement scheme, deformation occurred when the middle nodes moved outward along the  $x$ -axis and the upper nodes generated only a small shrinkage displacement along the  $y$ -axis; even the bottom quadrilateral

panels generated bending along the diagonal direction. In the triangle enhancement scheme, deformation occurred when the upper nodes moved outward along the  $y$ -axis and generated no displacement along the  $x$ -axis.



**Fig. 14.** Overall deformation of 1-2

As shown in **Fig. 15** and **Fig. 16**, the deformation of the two structures in the second constraint case was similar to that in the first. In the quadrangle enhancement scheme, middle nodes moved outward along the  $x$ -axis, whereas in the triangle enhancement scheme, the upper nodes moved outward along the  $y$ -axis. The difference was that the bottom and the upper nodes both experienced shrinkage displacement along the  $y$ -axis in the quadrangle enhancement scheme.

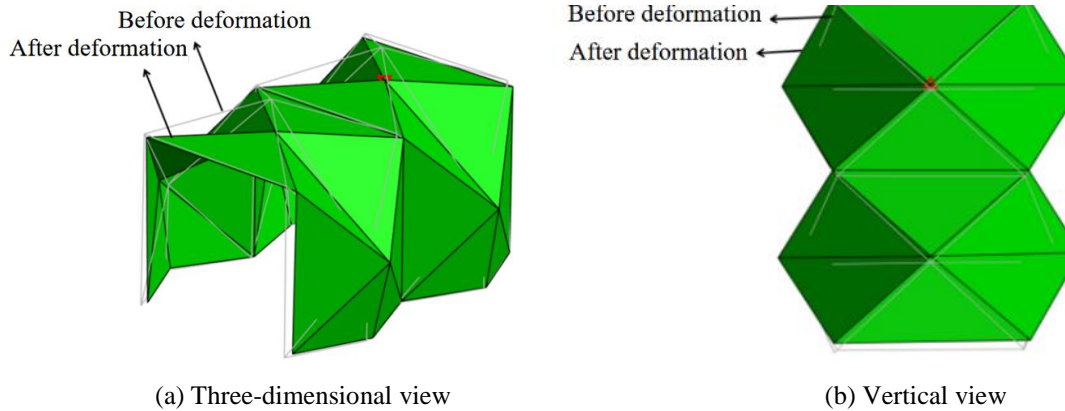


**Fig. 15.** Overall deformation of 2-1

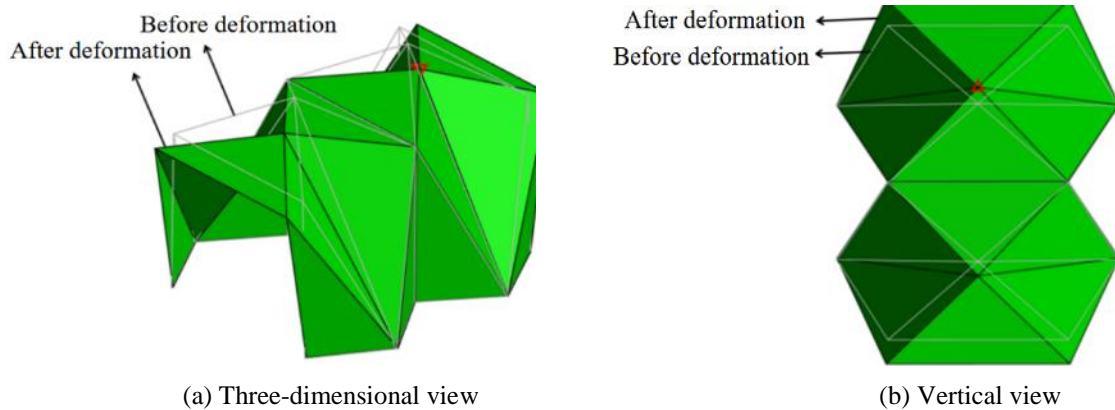


**Fig. 16.** Overall deformation of 2-2

The following **Fig. 17** and **Fig. 18** describe the developing process of applied load and stored energy by monitoring the displacement of the vertex. The red triangles in **Fig. 13- Fig.16** represent the monitoring point. In **Fig. 17**, 1-1 had a maximum load of  $28.0 \times 10^3$  kN, 1-2 had a maximum load of  $73.0 \times 10^3$  kN, 2-1 had a maximum load of  $26.6 \times 10^3$  kN, and 2-2 had a maximum load of  $72.9 \times 10^3$

kN. The triangle enhancement scheme could bear higher load. According to the line slope, the structural stiffness of the triangle was higher than that of the quadrilateral. Moreover, there was a similar maximum load between 1-2 and 2-2, which shows that the triangle enhancement had the structure self-constrained performance. In Fig. 18, 1-1 had a maximum stored energy of  $2.89 \times 10^6$  kJ, 2-1 had a maximum stored energy of  $2.76 \times 10^6$  kJ, 1-2 had a maximum stored energy of  $7.47 \times 10^6$  kJ, and 2-2 had a maximum stored energy of  $7.46 \times 10^6$  kJ, which constituted a similar result as Fig. 17. For a structure bearing the same load or storing the same amount of energy, the deformation of a triangle was much smaller than that of a quadrilateral.

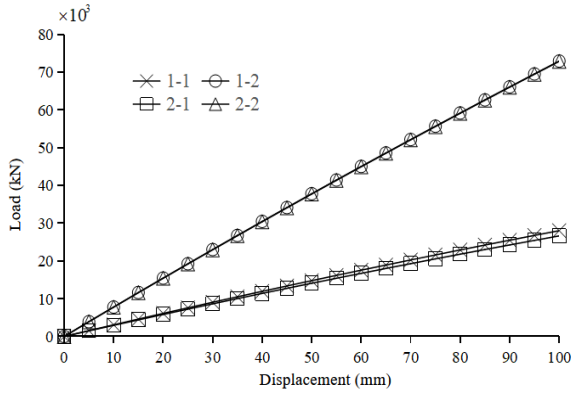


Fig. 17. Displacement-load

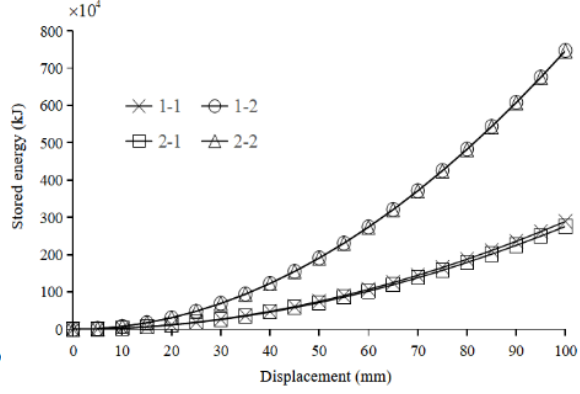


Fig. 18. Displacement-stored energy

#### 4.4 Failure modes

Subsequently compared the failure types of the two enhancement schemes when all bottom nodes were fully consolidated and a vertical displacement of 1.5 m was applied to the two nodes at the top of the structure. First, observing the 3D structure of the quadrangle enhancement scheme shown in Fig. 19a, it is found that the middle nodes moved outward along the  $x$ -axis and the upper nodes generated only a small shrinkage displacement along the  $y$ -axis; even the bottom quadrilateral panels generated bending along the diagonal direction. The overall failure mechanism could be divided into four stages: OA, AB, BC, and CD. OA was the elastic stage, where the stiffness of the structure remained the same; AB was the plastic stage, where the structural stiffness decreased gradually with the increase in displacement and where a maximum bearing capacity of  $81.5 \times 10^3$  kN was achieved at point B; BC was the decline stage, where the bearing capacity of the structure gradually decreased with displacement; and CD was the structure failure stage, where the structure failed despite still having some carrying capacity. The quadrangle enhancement scheme exhibited plastic failure.

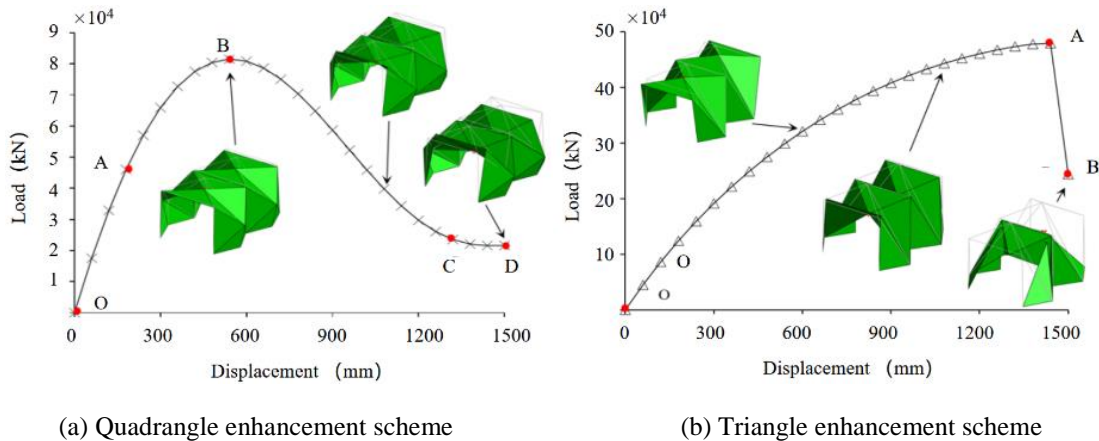


Fig. 19. Structure failure type

Then observed the 3D structure of the triangle enhancement scheme shown in Fig. 19b. The upper nodes moved outward along the  $y$ -axis with the top two nodes of vertical displacement changing. When the top nodes dropped to the same horizontal plane as the upper node, the upper nodes began to shrink

and move inward along the  $y$ -axis. Finally, the structure was suddenly destroyed. In the OA section in Fig. 19b, the structural stiffness decreased gradually with displacement, reaching a maximum of  $479.5 \times 10^3$  kN at point A; the structure was directly damaged and lost its bearing capacity in the AB section. The triangle enhancement scheme exhibited brittle failure.

Through the analysis of two different bottom constraints and structural failure forms, it is seen that the maximum load of the quadrilateral enhancement scheme was far less than that of the triangular enhancement scheme and that the quadrilateral panel at the bottom produced bending, which resulted in the irregular deformation of the structure. The triangle had a structure with self-constrained performance and better stability. Therefore, under the same conditions, the triangular reinforcement scheme was more recommended, but the maximum load should be calculated to prevent brittle damage.

#### 4.5 Connection hinge

Establishing suitable connections is a key consideration in the use of an origami structure. If no suitable connection exists after a new structural form was proposed, the design cannot be practically applied. The ordinary hinge was used to achieve rotation by driving the tapping screw into the plate from a direction parallel to the plate surface, but this type of connection may weaken the mechanical performance of CLT material, which will have a great impact on the load-bearing performance of the origami structure. Proper connections are in need to reduce the damage to the CLT plate and improve the accuracy of the mathematical analysis. For this reason, a new connection method was proposed in this paper.

The new hinge connection between plates was constituted by several steel components (Fig.20): two-channel sections, four bolts, and a hinge. The two-channel sections could rotate through the hinge. Then the two plates were respectively put into the channel steel and fixed by bolts to realize the hinge connection between the plates.

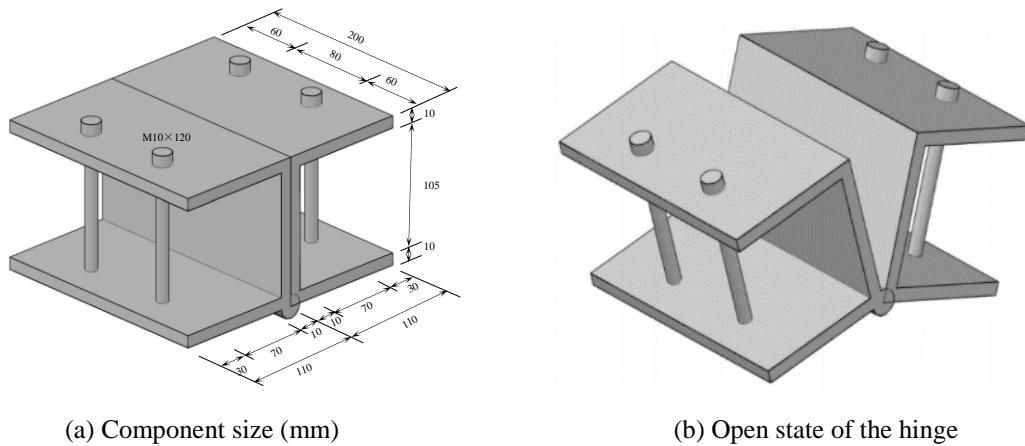


Fig. 20. Steel component

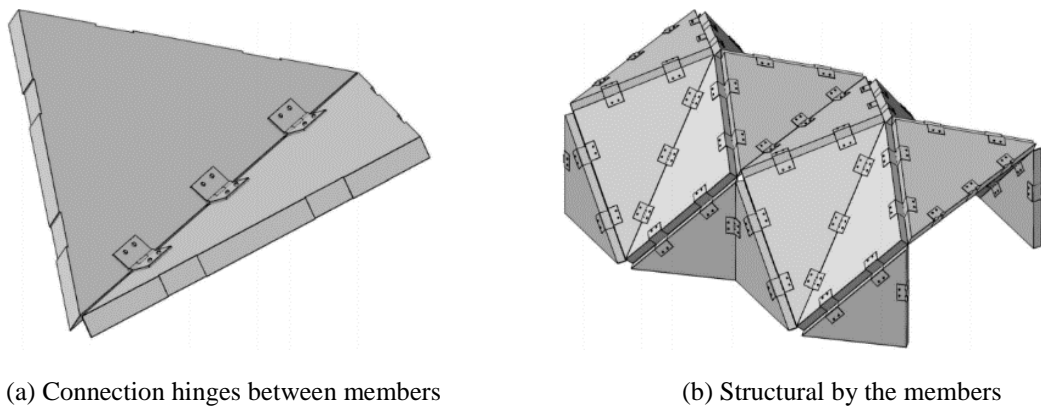


Fig. 21. Member and Connection

The practical application of the hinge was illustrated in **Fig. 21**. The hinge facilitated the rotation between plates and reduces damage to the strength of the plates, and its size was determined according to the size of CLT plate in the origami structure.

## 5 Conclusion

This study presented parametric design of developable wood structure based on Yoshimura origami pattern. The following conclusions were drawn:

1) The number of DOFs was simplified. In this paper, a complete set of constraint equations was constructed, through which the DOF of Yoshimura origami pattern was reduced from 6 to 3 and finally to 1, so that the Jacobi matrix of single vertex Yoshimura origami pattern could be obtained, which greatly reduces the computational workload and complexity.

2) The interaction between the plane angled  $\alpha$  and dihedral angle  $\theta$  based on the Yoshimura origami pattern was determined. The dihedral angle  $\theta$  increases as the plane angle  $\alpha$  of the crease pattern increase; however, the gradient of increase gradually decreases. For the same plane angle  $\alpha$ , increasing the number of valleys increases the dihedral angle  $\theta$ , and for a certain number of valleys, the design of the plane angle  $\alpha$  was not only limited by the maximum value of  $45^\circ$  but also by the minimum value.

3) Two strengthening schemes were proposed, and the deformation, failure mode and bearing capacity of the structure under these two strengthening schemes were investigated. The failure form of the quadrilateral reinforcement scheme was plastic failure, and the triangular reinforcement scheme was brittle failure. However, the load-bearing capacity and resistance to deformation of the triangular reinforcement scheme were much greater than that of the quadrilateral reinforcement scheme, so the triangular reinforcement scheme was recommended.

4) A connection method suitable for CLT material was designed. CLT material was high-strength, green and environment-friendly, and had excellent mechanical properties. Therefore, this paper used CLT material to design origami structure, as well as designed a new hinge connection for such CLT origami structure, which reduced the damage of hinge to material and facilitated the rotation between plates.

However, only mathematical analysis of the structure was performed in this paper, specific tests are in need to prove the feasibility of the CLT origami structure as well as the new connection method. In the future, further study will be taken to optimize this structure and improve its practicality.

## Funding Statement

This study was supported by “the Fundamental Research Funds for the Central Universities in China (2021ZY53)”

## Conflicts of Interest

The authors declare that they have no conflicts of interest to report regarding the present study.

## References

- [1] He ZY. On the foldability of rigid origami. 2021. <https://doi.org/10.17863/CAM.80207>
- [2] Feng HJ; Peng R; Zang SX; Ma JY; Chen Y. Rigid foldability and mountain-valley crease assignments of square-twist origami pattern. *Mechanism and Machine Theory* 2020; 152. <https://doi.org/10.1016/j.mechmachtheory.2020.103947>
- [3] Koizumi M. FGM activities in Japan. *Composites Part B: Engineering* 1997; 28(1-2): 1-4.
- [4] Kuribayashi K, Tsuchiya K, You Z, Tomus D, Umemoto M, Ito T, Sasaki M. Self-deployable origami stent grafts as a biomedical application of Ni-rich TiNi shape memory alloy foil. *Materials Science and Engineering: A* 2005; 419(1-2): 131-137. <https://doi.org/10.1016/j.msea.2005.12.016>
- [5] Miura K. Method of Packaging and Deployment of Large Membranes in Space. *Institute of Space & Astronautical Science Report*; 1985(618): 1-9.
- [6] Huffman, David A. Curvature and Creases: A Primer on Paper. *IEEE Transactions on Computers* 1976; C-25(10): 1010-9.
- [7] Stavric MAW, Bogensperger T. Generative Design for Folded Timber Structures. *CAADRIA 2015 - 20th International Conference on Computer-Aided Architectural Design Research in Asia: Emerging Experiences in the Past, Present and Future of Digital Architecture* 2015: 673-682.

- [8] Andreas F, Peter VB, Poul Henning K. Folded plate structures as building envelopes. World Conference on Timber Engineering 2012. 2012: 155-164
- [9] Guest SD, Pellegrino S. The Folding of Triangulated Cylinders, Part I: Geometric Considerations. *J Appl Mech* 1994; 61(4): 773-777. <https://doi.org/10.1115/1.2901553>
- [10] Guest SD, Pellegrino S. The Folding of Triangulated Cylinders, Part II: The Folding Process. *J Appl Mech* 1994; 61(4): 778-783. <https://doi.org/10.1115/1.2901554>
- [11] Guest SD, Pellegrino S. The Folding of Triangulated Cylinders, Part III: Experiments. *J Appl Mech* 1996; 63(1): 77-83. <https://doi.org/10.1115/1.2787212>
- [12] Hunt GW, Ario I. Twist buckling and the foldable cylinder: an exercise in origami. *International Journal of Non-Linear Mechanics* 2005; 40(6): 833-843. <https://doi.org/10.1016/j.ijnonlinmec.2004.08.011>
- [13] Yang K, Xu SQ, Shen J, Zhou SW; Xie YM. Energy absorption of thin-walled tubes with pre-folded origami patterns: Numerical simulation and experimental verification. *Thin-Walled Struct* 2016; 103: 33-44. <https://doi.org/10.1016/j.tws.2016.02.007>
- [14] Yang K, Xu SQ, Zhou SW, Xie YM. Multi-objective optimization of multi-cell tubes with origami patterns for energy absorption. *Thin-Walled Struct* 2018; 123: 100-113. <https://doi.org/10.1016/j.tws.2017.11.005>
- [15] Ma JY, Hou DG, Chen Y, You Z. Quasi-static axial crushing of thin-walled tubes with a kite-shape rigid origami pattern: Numerical simulation. *Thin-Walled Struct* 2016; 100: 38-47. <https://doi.org/10.1016/j.tws.2015.11.023>
- [16] Hou DG, Chen Y, Ma JY, You Z. Axial Crushing of Thin-Walled Tubes with Kite-Shape Pattern. *Proceedings of the ASME Design Engineering Technical Conference and Computers and Information in Engineering Conference* 2015; 5B. <https://doi.org/10.1115/DETC2015-46671>
- [17] Shen WJ, Cao Y, Jiang XP, Zhang Z, Kremer GEO, Qin HT. Experimental and Numerical Investigation on Radial Stiffness of Origami-Inspired Tubular Structures. *J. Appl. Mech* 2022; 89(3): 031001. <https://doi.org/10.1115/1.4052799>
- [18] Zhang CC. Design and Experimental Study of Soft Robot Based on Origami Structure. Soochow University. 2020. DOI:10.27351/d.cnki.gszhu. 2020.003304.
- [19] Zhang QW, Xu J, Fang HB. Earthworm-Like Planar Locomotion Robot Based on Yoshimura-Origami Structure. *Proceedings of the ASME 2021 International Design Engineering Technical Conferences and Computers and Information in Engineering Conference*. 2021. <https://doi.org/10.1115/DETC2021-71868>
- [20] Matcha H, Ljubas A. Parametric Origami: Adaptable temporary buildings. *eCAADe 2010 Future Cities*. 2010.
- [21] Hani B, Yves W. ORIGAMI - Folded Plate Structures, Architecture. *Materials Science*. 2008.
- [22] Schenk M, Viquerat AD, Seffen KA, Guest SD. Review of Inflatable Booms for Deployable Space Structures: Packing and Rigidization. *Journal of Spacecraft and Rockets* 2014; 51: 762-778. <https://doi.org/10.2514/1.A.32598>
- [23] Cai JG, Qian ZL, Jiang C, Feng J, Xu YX. Mobility and Kinematic Analysis of Foldable Plate Structures Based on Rigid Origami. *J Mech Robot* 2016; 8(6): 064502. <https://doi.org/10.1115/1.4034578>
- [24] Filipov ET, Liu K, Tachi T, Schenk M, Paulino GH. Bar and hinge models for scalable analysis of origami. *International Journal of Solids and Structures* 2017; 124: 26-45. <https://doi.org/10.1016/j.ijsolstr.2017.05.028>
- [25] Liu K, Paulino GH. Nonlinear mechanics of non-rigid origami: An efficient computational approach. *Proceedings of the Royal Society A: Mathematical Physical and Engineering Sciences* 2017; 473. <https://doi.org/10.1098/rspa.2017.0348>.
- [26] Cherry R, Manalo A, Karunasena W, Stringer G. Out-of-grade sawn pine: A state-of-the-art review on challenges and new opportunities in cross laminated timber (CLT). *Construction and Building Materials* 2019; 211: 858-868. <https://doi.org/10.1016/j.conbuildmat.2019.03.293>.